

Accelerating the simulation of kinetic shear Alfvén waves with a dynamical low-rank approximation

Lukas Einkemmer^{a,*}

^aUniversity of Innsbruck, Austria

Abstract

We propose a dynamical low-rank algorithm for a gyrokinetic model that is used to describe strongly magnetized plasmas. The low-rank approximation is based on a decomposition into variables parallel and perpendicular to the magnetic field, as suggested by the physics of the underlying problem. We show that the resulting scheme exactly recovers the dispersion relation even with rank 1. We then perform a simulation of kinetic shear Alfvén waves and show that using the proposed dynamical low-rank algorithm a drastic reduction (multiple orders of magnitude) in both computational time and memory consumption can be achieved. We also compare the performance of robust first and second-order projector splitting, BUG (also called unconventional), and augmented BUG integrators as well as a FFT-based spectral and Lax–Wendroff discretization.

Keywords: dynamical low-rank approximation, kinetic Alfvén waves, gyrokinetics, complexity reduction, computer simulation

1. Introduction

Nuclear fusion promises clean, abundant, and cheap energy. While significant progress has been made over the last half century, there are still many challenges that remain (e.g. control of plasma instabilities and understanding turbulence and associated transport phenomena). Numerical simulations are one of the primary ways to gain insight into the behavior of such systems and to inform design decisions for future fusion devices.

However, many phenomena that are of interest (particularly in the edge and the scrape-off layer) require a kinetic description. Kinetic models are posed in a relatively high dimensional phase space (four dimensions for drift-kinetic type models, up to five dimensions for gyrokinetic models, and six dimensions for the full Vlasov equation). If this phase space is discretized directly the computational cost scales as $\mathcal{O}(n^d)$, where n is the number of grid points per dimension and d is the number of dimensions. This exponential increase of storage and computational cost is often referred to as the curse of dimensionality. It makes realistic simulations often prohibitively expensive. Thus, most commonly particle in cell (PIC) methods are employed in large scale codes (see, e.g., [52]). In this approach only the field quantities (which are at most three dimensional) are discretized and the kinetic behavior is resolved by particles dynamics. This, for some problems, can drastically reduce the computational effort needed, especially if high-performance computing systems are used. However, particle in cell methods suffer from numerical noise and slow convergence (as the square root in the number of particles). They are still drastically more expensive than fluid or magnetohydrodynamics simulations.

More recently, dynamical low-rank methods have been proposed in [19] to solve kinetic problems. These methods originate from early work in quantum mechanics [46, 41] and were later considered in a mathematical

*Corresponding author

Email address: lukas.einkemmer@uibk.ac.at (Lukas Einkemmer)

framework for ordinary differential equations (see, e.g., [35, 47]). In the latter context, many advances such as robust integrators [42, 5], rank adaptive methods [6, 7, 33, 32], and generalization to various tensor formats [43, 44, 45, 14, 4, 7] have been made. While such methods can be applied in a rather generic way to ordinary or partial differential equation, an efficient algorithm is only obtained if a suitable decomposition of variables is chosen that allows us to run the simulation with a small to moderate rank. For kinetic problems primarily a decomposition between spatial and velocity variables has been performed (see [16, 22, 23, 49, 48, 12, 8, 38]; some work on tensor decomposition also exists [36, 19, 1, 28]). It turns out that for kinetic problems this has a number of advantages. In particular, for collisional problems the associated fluid limit is often low-rank [12, 24] as are various linearized models of the Vlasov equation (e.g. Landau damping is a low-rank phenomenon [22]). Because of this, for many problems, dynamical low-rank approximation perform very well and drastically reduce the computational effort required. In some situations full six-dimensional kinetic simulations can be performed using a desktop computer [3]. One shortcoming of low-rank methods in the context of kinetic equation is that they are not conservative. However, recently, significant progress has been made to make such methods mass, momentum, and energy conservative [18, 27, 25].

Almost all of the previous work has been done in the context of the Vlasov–Poisson or Vlasov–Maxwell equations. For strongly magnetized plasmas (such as those found in fusion plasmas) using the Vlasov equation directly implies that we need to resolve the extremely fast cyclotron frequency. Thus, in this case analytically reduced models, called gyrokinetics, are most commonly used. While those retain the general structure of the Vlasov equation there are important differences. In this paper, our goal is to make the first step towards using dynamical low-rank simulations for strongly magnetized plasmas. A major change in this case is how the low-rank decomposition is done. Since in strongly magnetized plasmas the dynamics parallel and the perpendicular to the magnetic field often only weakly couples (this was already exploited in the Hasegawa–Wakatani standard model [31]), we decompose into variables perpendicular and parallel to the magnetic field. This, precisely because it respects the physics of the underlying problem, endows the proposed dynamical low-rank approximation with a number of advantageous properties, as we will show.

In this paper, we look at a gyrokinetic model with straight field lines that can be used to study kinetic shear Alfvén waves. After introducing the gyrokinetic model that we use (section 2) we will

- discuss in section 3 the chosen decomposition and derive the equations of motion for the dynamical low-rank approximation. A particularly important point here is the treatment of the vector potential. We will also discuss the time and space discretization used;
- show in section 4 that the proposed dynamical low-rank algorithm when applied to the kinetic Alfvén wave problem exactly reproduces the dispersion relation of the original problem. This is an important result as it shows us that, within the validity of linear theory, rank 1 is sufficient in order to obtain the correct behavior. It also allows us to understand why dynamical low-rank approaches work well in this case and justifies the decomposition chosen;
- in section 5 we present numerical simulation for kinetic Alfvén waves and compare them to analytic theory as well as a semi-Lagrangian simulation of the full problem. We observe excellent agreement and a drastic reduction in storage and computational cost. In section 6 we then compare different robust integrators and spatial discretization strategies as well as their respective computational cost.

2. Model equation

In this paper we will assume that the magnetic field lines are straight and point in the z -direction. This significantly simplifies the equations of gyrokinetics since the terms that describe the curvature of the magnetic field vanish. In non-dimensional form we obtain an evolution equation for the four-dimensional electron particle density function $f(t, x, y, z, v)$

$$\partial_t f + v \partial_z f + \frac{1}{M_e} (\partial_z \phi + \partial_t A) \partial_v f = 0, \quad (1)$$

where M_e is the ion to electron mass ratio and v is the velocity in the z -direction (no velocity component perpendicular to the magnetic field is taken into account here). Note that the equations have been non-dimensionalized with respect to the ion thermal speed $v_{th,i}$ and the length of the device L . This evolution equation couples to the z -component of the electric field $E_3 = -\partial_z\phi - \partial_t A$. Here the scalar potential is denoted by $\phi(t, x, y, z)$ and the z component of the vector potential is denoted by $A(t, x, y, z)$. The potentials are self-consistently determined by

$$(\partial_{xx} + \partial_{yy})\phi = C_P\rho \quad \text{and} \quad (\partial_{xx} + \partial_{yy})A = C_A j, \quad (2)$$

where the charge density and current are given by

$$\rho = 1 - \int f \, dv, \quad j = - \int v f \, dv$$

and

$$C_P = \frac{1}{(\rho_i/L)^2}, \quad C_A = \frac{\beta}{(\rho_i/L)^2}.$$

The plasma β (the ratio of plasma pressure to magnetic pressure) and ρ_i/L (the ratio between the ion gyroradius and the size of the device) are dimensionless parameters. For more details on this model we refer to [9, 40] and the gyrokinetic literature in general.

We note that although the structure of this equation is similar to the Vlasov–Poisson or Vlasov–Maxwell equations, there are important differences. The equation to determine the potential ϕ only has the part of the Laplacian that is perpendicular to the magnetic field (i.e. $\Delta_\perp = \Delta - \partial_{zz} = \partial_{xx} + \partial_{yy}$). Thus, for each point in z we solve independent 2D dimensional Poisson problems. The equation for the vector potential is similar. However, in the evolution equation (1) we actually need the time derivative, i.e. $\partial_t A$, and not the vector potential directly. This has some significant ramifications for the numerical schemes as well as the low-rank approximation proposed here.

3. Dynamical low-rank algorithm

The goal of this section is to detail the complexity reduction approach employed in this paper. Every complexity reduction approach for a dynamic system requires two ingredients; namely, an approximation of the high-dimensional quantities and a way to efficiently update them as the simulation progresses from one time step to the next.

We employ a low-rank approximation. In this approach the independent variables $\xi = (x, y, z, v)$ are separated into two groups $\xi = (\xi_1, \xi_2)$ and only functions that depend on either ξ_1 or ξ_2 are admitted in the low-rank representation. Such an approach has been shown to be effective for both kinetic equations that appear in plasma physics (such as the Vlasov–Poisson [19, 28] or Vlasov–Maxwell [22] equations) and in a number of transport problems (e.g. radiation transport problems [49, 12, 48, 37] or the Boltzmann–BGK equation [16, 24, 8]). In all of these cases ξ_1 contains the spatial variables and ξ_2 contains all the velocity variables. This reduces a six (or five) dimensional problem to a three-dimensional problem (although tensor approximations that further reduce the dimensionality of the problem have also been proposed [36, 19, 1, 28]). Besides numerical evidence, there are also physical reasons why such an approximation is effective. For example, we know that a low-rank structure exists in many important solutions to those equations; e.g. the collisional limit (see [12, 23, 24]) and physical phenomena that are described well by a linearization of the Vlasov equation (e.g. Landau damping [22] or the onset of the two-stream instability [3]) have a low-rank structure. Let us emphasize that, in general, the way this decomposition is done depends on the problem under consideration. For example, if a low-rank approximation is used e.g. in quantum mechanics [46, 41] or for the chemical master equation in biology [34, 50] the choice of the decomposition (and potentially also the choice of the tensor format) is very different.

In the present case we deal with plasmas that are strongly magnetized by an external magnetic field along the z -axis. The gyrokinetic approach removes the fastest scales associated with the cyclotron frequency,

which leads to equations (1) and (2). Those equations have significant differences compared to the classic electrostatic Vlasov–Poisson system. This is seen both in the field equations, where only $\Delta_{\perp} = \partial_{xx} + \partial_{yy}$, i.e. the Laplacian perpendicular to the magnetic field appears, as well as in the evolution equation, where kinetic effects are only taken into account in the z -direction. The solution of such problems commonly admits a structure where the degrees of freedom associated with the z -direction can be separated from the perpendicular directions. This is not only the case for kinetic problems but is, e.g., also used in the Hasegawa–Wakatani standard model [31]. Thus, we consider here a decomposition with $\xi_1 = (x, y)$ and $\xi_2 = (z, v)$. The particle density function is then represented as

$$f(t, x, y, z, v) = \sum_{i=1}^r \sum_{j=1}^r X_i^f(t, x, y) S_{ij}^f(t) V_j^f(t, z, v), \quad (3)$$

where X_i^f , S_{ij}^f , and V_j^f are the corresponding low-rank factors (which depend only on (x, y) or (z, v) and are thus at most two dimensional). We assume the orthogonality conditions

$$\langle X_i^f, X_j^f \rangle_{xy} = \delta_{ij}, \quad \text{and} \quad \langle V_i^f, V_j^f \rangle_{zv} = \delta_{ij},$$

where $\langle f, g \rangle_{xy} = \int fg d(x, y)$ and $\langle f, g \rangle_{zv} = \int fg d(z, v)$ are the usual L^2 inner products. The rank of the approximation is denoted by r . Storing the full particle density would require $\mathcal{O}(n^4)$, where n is the number of grid points in each of the spatial and velocity directions, for simplicity here assumed to be equal. The low-rank approximation reduces this to $\mathcal{O}(rn^2)$. Increasing the rank increases the accuracy of the method. However, it also increases the storage and computational cost to run the simulation. We can also see from this discussion that using this decomposition, in the present case, is more appropriate than using $\xi_1 = (x, y, z)$ and $\xi_2 = (v)$, as this would still yield a three dimensional problem once the low-rank approximation has been performed and thus increase computational cost.

A major difference compared to the commonly used dynamical low-rank approximations for kinetic equations in the literature is that the field quantities are also subject to a low-rank approximation. That is, we consider

$$\phi(t, x, y, z) = \sum_{ij} X_i^{\phi}(t, x, y) S_{ij}^{\phi}(t) V_j^{\phi}(t, z), \quad \text{and} \quad \partial_t A(t, x, y, z) = \sum_{ij} X_i^{\partial_t A}(t, x, y) S_{ij}^{\partial_t A}(t) V_j^{\partial_t A}(t, z). \quad (4)$$

Note that in the algorithm we only use $\partial_t A$. The vector potential A is only used to compute the magnetic energy but otherwise does not need to be stored. From now on we will assume, if not indicated otherwise, that all summations run from 1 to r .

The second ingredient required in a complexity reduction scheme is a way to propagate the solution forward in time. For low-rank approximation there are two choices. First, one can start with a low-rank approximation and conduct a time step. This will increase the rank, by how much depends on the problem under consideration and the numerical method used. Then a truncation step is performed in order to reduce the rank to acceptable levels, see e.g. [36, 28]. This is often called the step-truncation approach. It should be emphasized that since the field quantities are also subject to a low-rank approximation, the situation here is quite different from the Vlasov–Poisson equation (for which the step-truncation approach has been considered in the references mentioned above). In our case a term like $\partial_z \phi \partial_v f$ has, in general, rank r^2 , while for the Vlasov–Poisson equation the electric field is not subject to a low-rank approximation and thus such a term is only of rank r . This, obviously, increases the memory required (in the intermediate steps) of a step-truncation approach.

We will use here the more recently developed dynamical low-rank approach [35, 19]. In this approach equations of motions for the low-rank factors are derived in the continuous setting which are then discretized (as any other PDE) using a numerical method. This has two primary advantages. First, the rank of the solution never increases and thus only approximations of rank r have to be stored. Second, it allows us to derive the low-rank approximation on the continuous level. This yields a set of PDEs to which we can then apply an appropriate numerical method. While we will here mainly use explicit integrators, for the equations

considered implicit approaches can be interesting [40]. Using an implicit scheme, e.g., is very hard in the step-truncation approach.

In the following we will consider the different parts of equations of motion separately. In section 3.1 we will consider the evolution equation (1). This is followed by the scalar potential ϕ in section 3.2 and the vector potential $\partial_t A$ in section 3.3. The details of the robust dynamical low-rank integrators are then discussed in section 3.4. Finally, we will consider the numerical discretization of the derived PDEs for the low-rank factors (section 3.5) and an adaptive time stepping algorithm (section 3.6).

3.1. Evolution equation

Applying the dynamical low-rank approach as described in [35, 19] results in a set of evolution equations that couple the low-rank factors X_i^f , S_{ij}^f , and V_j^f . In principle that system of equations can be integrated forward in time. However, it requires the computation of $(S^f)^{-1}$. For a sufficiently accurate approximation or even an overapproximation (i.e. where the rank is chosen larger than required) S^f has singular values which are close to zero and thus computing the inverse is ill-conditioned. Although, this problem has been known for a long time, the first robust dynamical low-rank integrator which does not suffer from this problem has been introduced relatively recently [42]. This projector-splitting integrator splits the projector onto the approximation space into three parts that correspond to the three low-rank factors. By doing so the three equations decouple which allows us to get rid of the ill-conditioned inverse (for a detailed discussion in the context of kinetic equations we refer to [19]). More recently, the basis updating Galerkin (BUG) integrator has been proposed in [5] and improved in [6]. The idea is different, but the BUG integrator still uses the same three evolution equations to perform the update. We will consider both integrators in the present work. How they combine the three equations outlined here in order to obtain an approximation to the dynamics is explained in section 3.4.

Equation for K : In the K step we consider not X_i by itself, but instead

$$K_j = \sum_i X_i S_{ij}.$$

This is a major ingredient that allows us to obtain a robust scheme. Note that we can always obtain X^f and S^f from K^f in a robust way by performing a QR decomposition. In order to obtain an evolution equation for K^f we project the dynamics of the equation onto the basis in $\xi_2 = (z, v)$ (i.e. onto the space spanned by the V_j^f). That is, we have

$$\partial_t K_j^f = \langle V_j^f, \text{RHS} \rangle_{zv},$$

where RHS is the right-hand side of equation (1). Thus, we have

$$\partial_t K_j^f = \langle V_j^f, -v \partial_z f - \frac{1}{M_e} (\partial_z \phi + \partial_t A) \partial_v f \rangle_{zv}.$$

Plugging in the low-rank representations for f , equation (3), ϕ , and $\partial_t A$, equation (4), we get

$$\begin{aligned} \partial_t K_j^f &= - \sum_l \langle v V_j^f, \partial_z V_l^f \rangle_{zv} K_l^f - \frac{1}{M_e} \sum_{ln} \left(K_n^\phi \langle (\partial_z V_n^\phi) V_j^f, \partial_v V_l^f \rangle_{zv} + K_n^{\partial_t A} \langle V_n^{\partial_t A} V_j^f, \partial_v V_l^f \rangle_{zv} \right) K_l^f \\ &= - \sum_l c_{jl}^1 K_l^f - \frac{1}{M_e} \sum_{ln} c_{jln}^2 K_n^\phi K_l^f - \frac{1}{M_e} \sum_{ln} c_{jln}^3 K_n^{\partial_t A} K_l^f, \end{aligned} \quad (5)$$

where the coefficients are given by

$$c_{jl}^1 = \langle v V_j^f, \partial_z V_l^f \rangle_{zv}, \quad c_{jln}^2 = \langle V_j^f \partial_v V_l^f, (\partial_z V_n^\phi) \rangle_{zv}, \quad c_{jln}^3 = \langle V_j^f \partial_v V_l^f, V_n^{\partial_t A} \rangle_{zv}.$$

Note that the coefficients are constant in time as only K^f (and thus X^f and S^f) are updated during this step. Thus, the coefficients c^1 , c^2 , and c^3 can be computed before performing the time stepping for equation

(5). Computing the coefficients is, however, a significant fraction of the overall run time of the algorithm. This is due to the fact that we have to compute multiple integrals of the basis functions and the scaling is not linear in r . For example, to store c_{jln}^2 requires only $\mathcal{O}(r^3)$ memory, but computing it has a cost of $\mathcal{O}(r^3n^2)$. Let us also emphasize that the equation for K is an ordinary differential equation. In particular, no spatial derivatives occur and thus this equation is easy to solve and parallelize.

Equation for S: In the S step we project onto both the space spanned by the X_i^f and the space spanned by the V_j^f . We have

$$\partial_t S_{ij}^f = \langle X_i^f V_j^f, \text{RHS} \rangle = -\langle X_i^f V_j^f, v \partial_z f + \frac{1}{M_e} (\partial_z \phi + \partial_t A) \partial_v f \rangle_{xyzv}.$$

Plugging in the low-rank representations for f , equation (3), ϕ , and $\partial_t A$, equation (3.3), and using the orthogonality relation between the basis functions, we get

$$\begin{aligned} \partial_t S_{ij}^f &= -\sum_l S_{il}^f \langle v V_j^f, \partial_z V_l^f \rangle_{xyzv} - \frac{1}{M_e} \sum_{mnl} S_{kl}^f \langle X_i^f, X_m^\phi X_k^f \rangle_{xy} S_{mn}^\phi \langle (\partial_z V_n^\phi) V_j^f, \partial_v V_l^f \rangle_{zv} \\ &\quad - \frac{1}{M_e} \sum_{mnl} S_{kl}^f \langle X_i^f, X_m^{\partial_t A} X_k^f \rangle_{xy} S_{mn}^{\partial_t A} \langle V_n^{\partial_t A} V_j^f, \partial_v V_l^f \rangle_{zv} \\ &= -\sum_l S_{il}^f c_{jl}^1 - \frac{1}{M_e} \sum_{nk} \left(\sum_m d_{ikm}^2 S_{mn}^\phi \right) \left(\sum_l S_{kl}^f c_{jln}^2 \right) - \frac{1}{M_e} \sum_{nk} \left(\sum_m d_{ikm}^3 S_{mn}^{\partial_t A} \right) \left(\sum_l S_{kl}^f c_{jln}^3 \right), \end{aligned} \quad (6)$$

where

$$d_{ikm}^2 = \langle X_i^f, X_k^f X_m^\phi \rangle_{xy}, \quad d_{ikm}^3 = \langle X_i^f, X_k^f X_m^{\partial_t A} \rangle_{xy}.$$

Once again this is an ordinary differential equation with coefficients that are constant in time during that step. Since S has only r^2 entries, solving equation (6) is only a negligible part of the overall computational cost of the algorithm.

Equation for L: In the L step we consider

$$L_i = \sum_j S_{ij} V_j.$$

Once again we can easily obtain S^f and V^f from L^f by performing a QR decomposition. We proceed in the same way as before, except that we now project onto the basis in $\xi_1 = (x, y)$, i.e. onto the space spanned by the X_i^f . We have

$$\partial_t L_i^f = \langle X_i^f, \text{RHS} \rangle_{xy}.$$

Plugging in the low-rank representations for f , equation (3), ϕ , and $\partial_t A$, equation (4), and using the orthogonality relation between the basis functions, we get

$$\begin{aligned} \partial_t L_i^f &= \langle X_i^f, -v \partial_z f - \frac{1}{M_e} (\partial_z \phi + \partial_t A) \partial_v f \rangle_{xy} \\ &= -v \partial_z L_i^f - \frac{1}{M_e} \sum_{mk} \langle X_i^f, X_m^\phi X_k^f \rangle_{xv} (\partial_z L_m^\phi) \partial_v L_k^f - \frac{1}{M_e} \sum_{mk} \langle X_i^f, X_m^{\partial_t A} X_k^f \rangle_{xv} L_m^{\partial_t A} \partial_v L_k^f \\ &= -v \partial_z L_i^f - \frac{1}{M_e} \sum_k (e_{ik} + e_{ik}^A) \partial_v L_k^f, \end{aligned} \quad (7)$$

where

$$e_{ik}(z) = \sum_m d_{ikm}^2 \partial_z L_m^\phi(z), \quad e_{ik}^A(z) = \sum_m d_{ikm}^3 L_m^{\partial_t A}(z).$$

Note that we can also use $e_{ik} = \langle X_i^f(\partial_z \phi) X_k^f \rangle_{xy}$ and $e_{ik}^A = \langle X_i^f(\partial_t A) X_k^f \rangle_{xy}$. However, computing these quantities by using d^2 and d^3 (which for both the projector splitting and unconventional integrator can be reused from a previous step in the algorithm) is more efficient.

Note that the free streaming term is treated exactly by the low-rank approximation. That is, no approximation is made to this term in equation (7). This makes sense as this is an advection in z with a speed that only depends on v and thus this term only depends on variables in $\xi_2 = (z, v)$. For the second term in equation (7) the primary approximation made is due to the fact that we also have to perform a low-rank approximation of the field quantities. The result is still an advection in v , but with a, in general, approximated velocity owing to the fact that we can not represent the field quantities exactly.

3.2. Equation for the scalar potential

In order to determine the scalar potential we have to solve the following Poisson problem for each z coordinate

$$(\partial_{xx} + \partial_{yy})\phi = C_P \rho.$$

Note that due to the separation of the dynamics parallel and perpendicular to the magnetic field this differential operator only acts in $\xi_1 = (x, y)$. This makes it perfectly compatible with the low-rank approximation that we employ here. Plugging in the low-rank expansion for ϕ and f we get

$$\sum_j \left((\partial_{xx} + \partial_{yy}) K_j^\phi \right) V_j^\phi = C_P \left(1 - \sum_j K_j^f \langle V_j^f \rangle_v \right), \quad \langle f \rangle_v = \int f dv.$$

Note that $\langle V_j^f \rangle_v$ is not an orthonormal basis (V_j^f is, but since we integrate in v this property is lost). However, we can easily find a basis for the right-hand side of the equation by orthonormalizing $(1, \langle V_1^f \rangle_v, \dots, \langle V_r^f \rangle_v)$. If we call the resulting orthonormal basis V_j^ρ we have

$$\rho = \sum_{j=1}^{r+1} \rho_j V_j^\rho, \quad \rho_j = \langle \rho, V_j^\rho \rangle_z.$$

This relation is exact since f has a low-rank structure and thus the same is true for ρ . The rank increases by at most 1 to $r+1$. We can also explicitly calculate ρ_j from the low-rank representation of f . We have

$$\begin{aligned} \rho_j &= \langle \rho, V_j^\rho \rangle_z \\ &= \langle 1, V_j^\rho \rangle_z - \sum_i K_i^f \left\langle V_j^\rho, \langle V_i^f \rangle_v \right\rangle_z. \end{aligned}$$

If a QR decomposition is used to compute (note that the QR decomposition is formulated here in the continuous setting; once a discretization has been performed this becomes a classic QR decomposition)

$$\sum_l V_l^\rho R_{li} = \left(1, \langle V_1^f \rangle_v, \dots, \langle V_r^f \rangle_v \right)_i$$

we have

$$\rho_j = \|1\|_z \delta_{j1} - \sum K_i^f R_{j,i+1}.$$

Since we now have an orthonormal basis we can choose $V_j^\phi = V_j^\rho$ which implies at once

$$(\partial_{xx} + \partial_{yy}) K_j^\phi = \rho_j. \quad (8)$$

Thus, we have to solve at most $r+1$ two-dimensional Poisson problems in (x, y) . Any Poisson solver can be used to do that. For a fast Poisson solver that scales linearly in the number of unknowns, the computational cost is $\mathcal{O}(rn^2)$. We note that this is usually significantly lower compared to computing the coefficients and integrating the evolution equations (the steps discussed in the previous section). Thus, this step, if implemented in the way suggested, only adds a negligible amount of compute time to the algorithm.

3.3. Iterative scheme for $\partial_t A$

It is easy to compute the vector potential A in a similar way as was described for the scalar potential in the previous section. It also satisfies a Poisson equation in (x, y) with the primary difference being that the right-hand side is given by the current and not the charge density. However, in the evolution equation (1) we do not require A , but $\partial_t A$. We could approximate $\partial_t A$ by forward differences which, since f at the next time point is not known, would result in an implicit scheme that couples f and $\partial_t A$, which is computationally expensive.

However, we can also derive an equation that directly relates $\partial_t A$ to quantities of the particle density function at the same point in time. By taking the time derivative of

$$(\partial_{xx} + \partial_{yy})A = C_A j$$

we get

$$(\partial_{xx} + \partial_{yy})\partial_t A = C_A \partial_t j. \quad (9)$$

We can now express $\partial_t j$ using equation (1) to get

$$\partial_t j = - \int v \partial_t f dv = \partial_z \int v^2 f dv - \frac{1}{M_e} (\partial_z \phi + \partial_t A) (1 - \rho).$$

Rearranging equation (9) we get

$$\left(\partial_{xx} + \partial_{yy} + \frac{C_A}{M_e} (1 - \rho) \right) \partial_t A = C_A \partial_z \int v^2 f dv - \frac{C_A}{M_e} (\partial_z \phi) (1 - \rho). \quad (10)$$

This is still a symmetric operator. Thus, we can apply a conjugate gradient method to find the solution. Conjugate gradient only requires the evaluation of the operator applied to an arbitrary vector. For the differential part this can be done easily as

$$(\partial_{xx} + \partial_{yy})\partial_t A = \sum_{ij} (\partial_{xx} + \partial_{yy}) X_i^{\partial_t A} S_{ij}^{\partial_t A} V_j^{\partial_t A}.$$

However, the addition or multiplication of two rank r functions is, in general, not a rank r function. Thus, we need to multiply $\partial_t A$ and $1 - \rho$ together and then add it to the result of applying the differential operator, which increases the rank to at most $r + r^2$. Then we perform a truncation back to rank r using a singular value decomposition. Since the singular value decomposition only needs to be performed for S this can be done very efficiently. Nevertheless, since at least a couple of iterations are required for convergence, this procedure has to be done multiple times in each time step and thus computing $\partial_t A$ can still be a significant fraction of the overall run time of the algorithm. We note, however, that $\partial_t A$ does not depend on v and thus the additional memory required to store intermediate results is much lower than for a step-truncation algorithm (where the same would need to be done for f). This is, in particular, true for the examples we consider in this paper, where significantly more grid points are required in the v direction compared to the spatial directions.

We also need to compute the right-hand side of equation (10). We have $\partial_z \int v^2 f dv$ which is of rank r . The term $(\partial_z \phi)(1 - \rho)$ has (at most) rank $\mathcal{O}(r^2)$ since we multiply two terms of rank $\mathcal{O}(r)$ together. Thus, in total the right-hand side has (at most) rank $\mathcal{O}(r^2 + r)$. We perform those operations and truncate them using a singular value decomposition (as above). Since this is only done once, the computational cost is usually only a very small part of the overall algorithm.

3.4. Dynamical low-rank algorithm

In principle we can solve the coupled equations for the low-rank factors (5), (6), and (7) of f together with the equations for the potentials (8) and (10) to obtain the solution. However, in order to do so we have to

invert S , since equation (5) is formulated in terms of K (and not X) and equation (7) is formulated in terms of L (and not V). This, however, is undesirable as in cases where the smallest singular value of S is small the inverse of S is ill-conditioned. If the smallest singular value of S becomes larger, however, the approximation is usually very inaccurate (as we neglect singular values that are relatively large and thus important).

In order to remedy this problem integrators that are robust to the presence of small singular values have been developed. In particular, the projector splitting integrator [42] and the recently developed class of basis updating Galerkin (BUG) integrators [5, 6] (also called unconventional integrators) have this property. The only difference is how those algorithm combine equations (5), (6), and (7) in order to update the numerical solution. In both cases, in order to increase computational efficiency, we split the field solves from the time update. The first order projector splitting integrator is shown in Algorithm 1, the first order BUG integrator is shown in Algorithm 2, and an augmented version of the BUG integrator (as described in [6]) is shown in Algorithm 3. For more details on the projector splitting and BUG integrator, specifically in the context of kinetic problems, we refer the reader to [19] and [37], respectively. We also note that since the projector splitting integrator is a splitting scheme it can be raised to higher order (see, e.g., [19, 3]). The primary difficulty here is that it is not sufficient to compute the (frozen) field quantities only at the beginning of the time step. However, we know from [21, 20] that if we have a first order approximation of the field quantities at the half step (i.e. at $t^{n+1/2} = t^n + \Delta t/2$) then applying a Strang splitting scheme using those field quantities retains second order accuracy. We thus first perform a Lie splitting step to obtain a first order approximation at the half step, from which the field quantities that are then used in the Strang splitting are determined. The second order projector splitting integrator based on this idea is shown in Algorithm 4. Let us also note that there is currently no second order variant of the BUG integrator.

Algorithm 1 First order Lie projector splitting integrator with time step size $\Delta t = t^{n+1} - t^n$, where t^n is the time at the beginning of the current step and t^{n+1} is the time at the end of the current step. Note that the S step is integrated backward in time.

Input: X_i^n, S_{ij}^n, V_j^n such that $f(t^n, x, y, z, v) \approx \sum_{ij} X_i^n(x, y) S_{ij}^n V_j^n(z, v)$

Output: $X_i^{n+1}, S_{ij}^{n+1}, V_j^{n+1}$ such that $f(t^{n+1}, x, y, z, v) \approx \sum_{ij} X_i^{n+1}(x, y) S_{ij}^{n+1} V_j^{n+1}(z, v)$

1. Solve the Poisson problem (8) to obtain $K_j^{\phi, n}$ and $V_j^{\phi, n}$ (i.e. ϕ^n) from f^n .
 2. Iteratively solve equation (10) to obtain $X_i^{\partial_t A, n}, S_{ij}^{\partial_t A, n}$, and $V_j^{\partial_t A, n}$ (i.e. $\partial_t A^n$) from f^n and ϕ^n .
 3. (K step) Perform a time step using time step size Δt and equation (5) with initial value $\sum_i X_i^n S_{ij}^n$ to obtain K_j^* .
 4. Perform a QR decomposition of K_j^* to obtain $X_i^{n+1} = Q$ and $S_{ij}^* = R$.
 5. (S step) Perform a time step using time step size $-\Delta t$ and equation (6) with initial value S_{ij}^* to obtain S_{ij}^{**} .
 6. (L step) Perform a time step using time step size Δt and equation (7) with initial value $\sum_j S_{ij}^{**} V_j^n$ to obtain L_i^* .
 7. Perform a QR decomposition of L_i^* to obtain $V_j^{n+1} = Q$ and $S_{ij}^{n+1} = R$.
-

Algorithm 2 BUG integrator with time step size $\Delta t = t^{n+1} - t^n$, where t^n is the time at the beginning of the current step and t^{n+1} is the time at the end of the current step.

Input: X_i^n, S_{ij}^n, V_j^n such that $f(t^n, x, y, z, v) \approx \sum_{ij} X_i^n(x, y) S_{ij}^n V_j^n(z, v)$

Output: $X_i^{n+1}, S_{ij}^{n+1}, V_j^{n+1}$ such that $f(t^{n+1}, x, y, z, v) \approx \sum_{ij} X_i^{n+1}(x, y) S_{ij}^{n+1} V_j^{n+1}(z, v)$

1. Solve the Poisson problem (8) to obtain $K_j^{\phi, n}$ and $V_j^{\phi, n}$ (i.e. ϕ^n) from f^n .
 2. Iteratively solve equation (10) to obtain $X_i^{\partial_t A, n}, S_{ij}^{\partial_t A, n}$, and $V_j^{\partial_t A, n}$ (i.e. $\partial_t A^n$) from f^n and ϕ^n .
 3. (K step) Perform a time step using time step size Δt and equation (5) with initial value $\sum_i X_i^n S_{ij}^n$ to obtain K_j^* .
 4. Perform a QR decomposition of K_j^* to obtain $X_i^{n+1} = Q$ and throw away R .
 5. (L step) Perform a time step using time step size Δt and equation (7) with initial value $\sum_j S_{ij}^n V_j^n$ to obtain L_i^* .
 6. Perform a QR decomposition of L_i^* to obtain $V_j^{n+1} = Q$ and throw away R .
 7. Compute $M_{ik} = \langle X_i^{n+1}, X_k^n \rangle_{xy}$ and $N_{jl} = \langle V_j^{n+1}, V_l^n \rangle_{zv}$.
 8. Recompute $c_{jl}^1, c_{jln}^2, c_{jln}^3, d_{ikm}^2, d_{ikm}^3$ using X_i^{n+1} and V_j^{n+1} .
 9. (S step) Perform a time step using time step size Δt and equation (6) with initial value $\sum_{kl} M_{ik} S_{kl}^n N_{jl}$ and the coefficients computed in step 8 to obtain S_{ij}^{n+1} .
-

Algorithm 3 Augmented BUG integrator with time step size $\Delta t = t^{n+1} - t^n$, where t^n is the time at the beginning of the current step and t^{n+1} is the time at the end of the current step. For the orthogonalization an arbitrary algorithm (e.g. modified Gram–Schmidt) can be employed. Note, however, that for the method described we assume that the orthogonalization algorithm does not change the first r basis vectors (which are already orthogonal). This makes the computation of of the initial value for the S step trivial.

Input: X_i^n, S_{ij}^n, V_j^n such that $f(t^n, x, y, z, v) \approx \sum_{ij} X_i^n(x, y) S_{ij}^n V_j^n(z, v)$

Output: $X_i^{n+1}, S_{ij}^{n+1}, V_j^{n+1}$ such that $f(t^{n+1}, x, y, z, v) \approx \sum_{ij} X_i^{n+1}(x, y) S_{ij}^{n+1} V_j^{n+1}(z, v)$

1. Solve the Poisson problem (8) to obtain $K_j^{\phi, n}$ and $V_j^{\phi, n}$ (i.e. ϕ^n) from f^n .
2. Iteratively solve equation (10) to obtain $X_i^{\partial_t A, n}, S_{ij}^{\partial_t A, n}$, and $V_j^{\partial_t A, n}$ (i.e. $\partial_t A^n$) from f^n and ϕ^n .
3. (K step) Perform a time step using time step size Δt and equation (5) with initial value $\sum_i X_i^n S_{ij}^n$ to obtain K_j^* .
4. Perform a QR decomposition of K_j^* to obtain $X_i^* = Q$ and throw away R .
5. (L step) Perform a time step using time step size Δt and equation (7) with initial value $\sum_j S_{ij}^n V_j^n$ to obtain L_i^* .
6. Perform a QR decomposition of L_i^* to obtain $V_j^* = Q$ and throw away R .
7. Form a new basis $X^{**} = \text{orthogonalize}([X^n, X^*])$ and $V^{**} = \text{orthogonalize}([V^n, V^*])$.
8. Recompute $c_{jl}^1, c_{jln}^2, c_{jln}^3, d_{ikm}^2, d_{ikm}^3$ using X^{**} and V^{**} .
9. (S step) Perform a time step using time step size Δt and equation (6) with initial value

$$S_{ij} = \begin{cases} S_{ij}^n & 1 \leq i \leq r, 1 \leq j \leq r \\ 0 & \text{otherwise} \end{cases}$$

and the coefficients computed in step 8 to obtain S_{ij}^{**} .

10. Perform an SVD to obtain $S_{ij}^{**} = \sum_k U_{ik} \sigma_k H_{kj}$.

11. Truncate the solution back to rank r by keeping only the r most important basis functions

$$\{S_{ij}^{n+1}\}_{i,j=1}^r = \delta_{ij} \sigma_i, \quad \{X_i^{n+1}\}_{i=1}^r = \sum_j X_j^{**} U_{ji}, \quad \{V_j^{n+1}\}_{i=1}^r = \sum_i H_{ji} V_i^{**}.$$

Algorithm 4 Second order Strang projector splitting integrator with time step size $\Delta t = t^{n+1} - t^n$, where t^n is the time at the beginning of the current step and t^{n+1} is the time at the end of the current step. Note that the S step is integrated backward in time.

Input: X_i^n, S_{ij}^n, V_j^n such that $f(t^n, x, y, z, v) \approx \sum_{ij} X_i^n(x, y) S_{ij}^n V_j^n(z, v)$

Output: $X_i^{n+1}, S_{ij}^{n+1}, V_j^{n+1}$ such that $f(t^{n+1}, x, y, z, v) \approx \sum_{ij} X_i^{n+1}(x, y) S_{ij}^{n+1} V_j^{n+1}(z, v)$

1. Apply Algorithm 1 using time step size $\Delta t/2$ and initial value X_i^n, S_{ij}^n, V_j^n to obtain $X_i^{n+1/2}, S_{ij}^{n+1/2}, V_j^{n+1/2}$.
 2. Solve the Poisson problem (8) to obtain $K_i^{\phi, n+1/2}$ and $V_j^{\phi, n+1/2}$ (i.e. $\phi^{n+1/2}$) from $X_i^{n+1/2}, S_{ij}^{n+1/2}, V_j^{n+1/2}$.
 3. Iteratively solve equation (10) to obtain $X_i^{\partial_t A, n+1/2}, S_{ij}^{\partial_t A, n+1/2}$, and $V_j^{\partial_t A, n+1/2}$ (i.e. $\partial_t A^{n+1/2}$) from $X_i^{n+1/2}, S_{ij}^{n+1/2}, V_j^{n+1/2}$ and $\phi^{n+1/2}$.
 4. (L step) Perform a time step using time step size $\Delta t/2$ and equation (7) with initial value $\sum_j S_{ij}^n V_j^n$ and $\phi^{n+1/2}, \partial_t A^{n+1/2}$ to obtain L_i^* .
 5. Perform a QR decomposition of L_i^* to obtain $V_j^* = Q$ and $S_{ij}^* = R$.
 6. (S step) Perform a time step using time step size $-\Delta t/2$ and equation (6) with initial value S_{ij}^* and $\phi^{n+1/2}, \partial_t A^{n+1/2}$ to obtain S_{ij}^{**} .
 7. (K step) Perform a time step using time step size Δt and equation (5) with initial value $\sum_i X_i^* S_{ij}^{**}$ and $\phi^{n+1/2}, \partial_t A^{n+1/2}$ to obtain K_j^* .
 8. Perform a QR decomposition of K_j^* to obtain $X_i^{n+1} = Q$ and $S_{ij}^{***} = R$.
 9. (S step) Perform a time step using time step size $-\Delta t/2$ and equation (6) with initial value S_{ij}^{***} and $\phi^{n+1/2}, \partial_t A^{n+1/2}$ to obtain S_{ij}^{****} .
 10. (L step) Perform a time step using time step size $\Delta t/2$ and equation (7) with initial value $\sum_j S_{ij}^{****} V_j^*$ and $\phi^{n+1/2}, \partial_t A^{n+1/2}$ to obtain L_i^{n+1} .
 11. Perform a QR decomposition of L_i^{n+1} to obtain $V_j^{n+1} = Q$ and $S_{ij}^{n+1} = R$.
-

A peculiarity of the projector splitting integrator is that it requires us to conduct the S step backward in time. For hyperbolic problems, such as the one we consider here, this is not an issue and simply means that we have to negate the right-hand side of equation (6). For both variants of the BUG integrator this is not necessary. However, from a computational point of view the BUG integrators are more expensive due to the need to recompute the coefficients with the new basis and, in the case of the augmented variant, to perform this computation and the S step for a basis with larger size ($2r$ instead of r). We will consider this computational aspects in more detail in section 6.

3.5. Numerical discretization

So far we have developed the dynamical low-rank approximation in the continuous setting (the approach introduced in [19]). That is, no time or space discretization has been performed yet. This has a number of advantages. First, it makes the distinction between the error due to the low-rank approximation and the error due to the spatial and temporal discretization clear. Second, since we start from a set of partial differential equations for the low-rank factors by providing an appropriate space and temporal discretization we can avoid the stability issues that in some cases arises if the numerical discretization is performed first [38]. Third, the numerical discretization can be tailored to the partial differential equations obtained for the low-rank factors. In this section we will detail the spatial and temporal discretization that we will use in our numerical simulations.

In order to solve for the scalar potential ϕ we employ a fast Fourier transform (FFT) based Poisson solver to obtain the solution of equation (8). In order to compute $\partial_t A$ we perform a conjugate gradient iteration to obtain a solution of equation (10). The spatial derivatives are computed using a FFT based approach.

The K equation (5) and S equation (6) are ordinary differential equations and thus require no spatial discretization. For the time integrator we employ the classic Runge–Kutta method of order 4.

The L equation (7) is a system of advection equations that depend on (z, v) . We consider two distinct ways to discretize this system.

Fourier spectral discretization: First we discretize L_i^f on an equidistant grid such that $L_{i;\alpha\beta}^f(t) \approx L_i^f(t, z_\alpha, v_\beta)$, where (z_α, v_β) denote the position of the equally spaced grid points. We then split equation (7) into

$$\partial_t L_i^f = -v \partial_z L_i^f \quad (11)$$

and

$$\partial_t L_i^f = -\frac{1}{M_e} \sum_k (e_{ik} + e_{ik}^A) \partial_v L_k^f. \quad (12)$$

Since in equation (11) the speed of the advection does not depend on the advection variables, we can easily solve this exactly in Fourier space (up to the truncation error of the Fourier series). This yields

$$L_{i;\beta}^f(\Delta t) = \text{FFT}^{-1} \left(\exp(-iv_\beta k_z \Delta t) \bullet \text{FFT}(L_{i;\beta}^f(0)) \right),$$

where k_z is the vector that contains all the frequencies in the z -direction and \bullet denotes the component-wise product of two vectors.

For equation (12) the situation is more complicated. This is primarily due to the fact that the different L_i^f couple to each other. However, since the matrix $E_{ik}(z) = e_{ik}(z) + e_{ik}^A(z)$ is symmetric (for each fixed z) we can diagonalize it, i.e.

$$\text{diag}(\lambda) = T^T E T.$$

Then we perform a coordinate transformation into the Eigenbasis

$$M_i^f = \sum_n T_{in}^T L_n^f.$$

which we use in equation (12) to obtain

$$\partial_t M_i^f = -\frac{1}{M_e} \lambda_i \partial_v M_i^f.$$

This can now be treated exactly (up to the truncation error) in Fourier space

$$M_{i;\alpha}^f(\Delta t) = \text{FFT}^{-1} \left(\exp(-i\lambda_{i;\alpha} k_v \Delta t / M_e) \bullet \text{FFT}(M_{i;\alpha}^f(0)) \right),$$

where k_v are the frequencies in the v -direction and we note that the eigenvalues depend on z and thus α once the discretization has been performed. We now have to simply undo the coordinate transformation to complete the algorithm and obtain $L_{i;\alpha\beta}^f(\Delta t)$.

We have chosen a Fourier spectral method here. However, it should be noted that any semi-Lagrangian method could be used in its place (as has commonly been done for kinetic problems; see, e.g., [51, 26, 39, 17]).

Lax–Wendroff discretization: As an alternative we can also employ a more traditional Lax–Wendroff scheme. For equation (11) this is immediate. For equation (12) we again change to the Eigenbasis and then apply the Lax–Wendroff method, i.e.

$$M_{i;\alpha\beta}^{f;1} = M_{i;\alpha\beta}^{f;0} - \frac{\Delta t}{2\Delta x} \frac{\lambda_{i\alpha}}{M_e} \left(M_{i;\alpha,\beta+1}^{f;0} - M_{i;\alpha,\beta-1}^{f;0} \right) + \frac{\Delta t^2}{2\Delta x^2} \frac{\lambda_{i\alpha}^2}{M_e^2} \left(M_{i;\alpha,\beta+1}^{f;0} - 2M_{i;\alpha\beta}^{f;0} + M_{i;\alpha,\beta-1}^{f;0} \right),$$

where $M_{i;\alpha\beta}^{f;1} \approx M_i^f(\Delta t, z_\alpha, v_\beta)$ and $M_{i;\alpha\beta}^{f;0} \approx M_i^f(0, z_\alpha, v_\beta)$.

3.6. Adaptive step size controller

In the numerical results presented in this paper we will use an adaptive step size controller. This has the advantage that the user is freed from choosing an appropriate time step size. For the standard approach we refer to [13, Chap. II.4] and [30], but note that it has been realized that, in particular, for implicit and exponential methods more efficient controllers can be constructed (see, e.g., [29, 2, 15, 10, 11]).

Since we use explicit and relatively low order methods here, we follow the classic idea of computing the solution once with time step Δt and once with time step $\Delta t/2$ and then estimating the error using Richardson extrapolation. An important question in this context is the appropriate metric for the error. We take the viewpoint that in many physical problems one is primarily interested in the evolution of macroscopic quantities and not necessarily in all of the details of the particle-density function. Thus, we consider for the step size controller the error in the electric and magnetic energy. This has the added benefit that those quantities can be computed from the low-rank representation at very low additional cost.

More specifically, the numerical scheme with time step size Δt yields a electric energy at time t^{n+1} denoted by $ee_{\Delta t}^{n+1}$ and a magnetic energy denoted by $me_{\Delta t}^{n+1}$, see equations (19) and (20) for a definition. Similar the numerical scheme applied twice with time step size $\Delta t/2$ yields electric energy at time t^{n+1} denoted by $ee_{\Delta t/2}^{n+1}$ and magnetic energy denoted by $me_{\Delta t/2}^{n+1}$. From this we can obtain an estimate using Richardson extrapolation

$$ee_{\text{RE}}^{n+1} = \frac{2^{p+1}ee_{\Delta t/2}^{n+1} - ee_{\Delta t}^{n+1}}{2^{p+1} - 1}, \quad me_{\text{RE}}^{n+1} = \frac{2^{p+1}me_{\Delta t/2}^{n+1} - me_{\Delta t}^{n+1}}{2^{p+1} - 1},$$

where the local truncation error of the scheme is assumed to be $\mathcal{O}(\Delta t^{p+1})$. We have $p = 2$ for the Strang based projector splitting and $p = 1$ for all other methods considered here. The Richardson extrapolated value has local truncation error of size $\mathcal{O}(\Delta t^{p+2})$ and can thus be used to estimate the error of $ee_{\Delta t/2}^{n+1}$ and $me_{\Delta t/2}^{n+1}$. We consider

$$\begin{aligned} (\text{err}^{n+1})^2 &= (ee_{\Delta t/2}^{n+1} - ee_{\text{RE}}^{n+1})^2 + (me_{\Delta t/2}^{n+1} - me_{\text{RE}}^{n+1})^2 \\ &= \frac{(ee_{\Delta t}^{n+1} - ee_{\Delta t/2}^{n+1})^2 + (me_{\Delta t}^{n+1} - me_{\Delta t/2}^{n+1})^2}{(2^{p+1} - 1)^2}. \end{aligned}$$

This is the absolute error. For the step size controller we use the relative error per unit time step. That is,

$$\text{rel_err_unit}^{n+1} = \frac{\text{err}^{n+1}}{\Delta t \sqrt{(ee_{\Delta t/2}^{n+1})^2 + (me_{\Delta t/2}^{n+1})^2}}.$$

The new step size is then determined according to the classic controller

$$\Delta t^{\text{new}} = \Delta t \left(s \frac{\text{tol}}{\text{rel_err_unit}^{n+1}} \right)^{1/(p+1)}, \quad (13)$$

where s is a safety factor ($s = 0.7$ is chosen in the numerical experiments). If $\text{rel_err_unit}^{n+1} > \text{tol}$ the step is rejected and the time step is repeated either with the new step size chosen according to equation (13) or half the previous time step, whichever of those two is smaller.

4. Properties of the dynamical low-rank algorithm

In order to show that the dynamical low-rank algorithm, for a given problem and initial value, works well, we need two ingredients. First, we need to show that the solution can be represented well by a low-rank approximation. That is, that (f, ϕ, A) can be approximated accurately by equations (3) and (4) with a

small rank r . Second, we need to show that the dynamical low-rank algorithm approximates this solution accurately. In this section we will show that this is the case if the dynamics is not too far from linear theory. We start by linearizing equation (1) at $(f, \phi, A) = (f_{eq}, 0, 0)$ and obtain

$$\partial_t f + v \partial_z f + \frac{1}{M_e} (\partial_z \phi + \partial_t A) \partial_v f_{eq} = 0, \quad (14)$$

where we again use f to denote the perturbation from f_{eq} . From this, the dispersion relation of the problem can be obtained (the detailed calculations can be found in Appendix A). The dispersion relation tells us that if initially a single spatial mode with wavenumber $k = (k_x, k_y, k_{\parallel})$ is excited, i.e. we consider the initial value

$$f(0, x, v) = (1 + \alpha \cos(k_x x) \cos(k_y y) \cos(k_{\parallel} z)) f_{eq}(v),$$

where f_{eq} is a Maxwellian and α is the strength of the perturbation, the solution at later time can be written as

$$f(t, x, v) = \text{Re}(1 + \alpha \exp(ik \cdot x - \omega t)) f_{eq}(v), \quad \phi(t, x) \propto \text{Re} \exp(ik \cdot x - \omega t), \quad A(t, x) \propto \text{Re} \exp(ik \cdot x - \omega t), \quad (15)$$

where ω is determined by

$$1 - \frac{2[1 + \bar{\omega} Z(\bar{\omega})]}{(k_{\perp} \rho_i / L)^2} (\beta / M_e \bar{\omega}^2 - 1) = 0, \quad \bar{\omega} = \sqrt{M_e} \frac{\omega}{k_{\parallel}}. \quad (16)$$

The important observation here is that this is a rank 1 solution. Thus, the solution has the correct structure to be approximated efficiently by equations (3) and (4).

However, this on its own is not sufficient. We also need that the dynamical low-rank algorithm, i.e. the equations of motions (5), (6), and (7), are able to capture this low-rank solution. Ideally, we want an algorithm that if the solution of our problem has a certain rank, say s , and we run the simulation with a rank $r \geq s$ then we obtain the exact result (up to time and space discretization errors).

For the dynamical low-rank approach this is indeed the case. In fact, we can write the dynamical low-rank approximation applied to equation (14) as

$$\partial_t f = P(f) \text{LIN}(f) = P(f) \left(-v \partial_z f - \frac{1}{M_e} (\partial_z \phi + \partial_t A) \partial_v f_{eq} \right), \quad (17)$$

where $P(f)$ is the orthogonal projector to the tangent space of functions with rank r (see, e.g., [35]). We also know that equation (15) is a solution to $\partial_t f = \text{LIN}(f)$. However, since f is rank 1, $\text{LIN}(f)$ lies in the corresponding tangent space and the projection operator is just the identity. That is, we have $P(f) \text{LIN}(f) = \text{LIN}(f)$ and the low-rank solution given by equation (15) is therefore also a solution of equation (17). Thus, within linear theory the low-rank algorithm is exact as the equations of motions (5), (6), and (7) are precisely the same as equation (17), only expressed in the low-rank factors X , S , and V instead of f .

We should duly note that this argument only applies to the dynamical low-rank algorithm as described in sections (3.1)-(3.3). In general, we have to apply a time and space discretization and those introduce numerical errors. However, this is also true for a direct discretization of the full problem. The only specific issue for dynamical low-rank approximations is that the robust integrators we use (see section 3.4) also introduces an additional time discretization error. This error tends to zero as Δt tends to zero (as is the case for any reasonable time discretization).

5. Alfvén waves

We will now use the proposed dynamical low-rank algorithm to simulate the propagation of kinetic shear Alfvén waves. We will also compare the results both to analytic theory (in cases where it applies) and a code

that directly discretizes the full four-dimensional problem, i.e. equation (1). As initial value we consider a Maxwellian equilibrium of the electrons that is perturbed in all spatial directions, i.e.

$$f(0, x, y, z, v) = (1 + \alpha \cos(k_x x) \cos(k_y y) \cos(k_{\parallel} z)) \frac{\exp(-M_e v^2)}{\sqrt{\pi/M_e}} \quad (18)$$

on the domain $(x, y, z, v) \in [0, 2\pi/k_x) \times [0, 2\pi/k_y) \times [0, 2\pi/k_{\parallel}) \times [-6/\sqrt{M_e}, 6/\sqrt{M_e})$. We use the physical mass ratio $M_e = 1/1830$ and choose $\beta/M_e = 1.8$. The wavevectors k_x , k_y , and k_z of the perturbation in the x , y , and z directions determine according to the dispersion relation (see Appendix A), assuming the linear theory holds true, the decay rate and frequency of the wave. We consider here $k_x = k_y = k_{\perp}/\sqrt{2}$ with $k_{\perp}\rho_i = 0.2$, $k_{\parallel} = 2\pi$, and $\alpha = 10^{-5}$. Note that for the dynamics only the value of the dimensionless parameter $k_{\perp}\rho_i$ is important and not how k_{\perp} and ρ_i is chosen individually. For this configuration the dispersion relation gives a decay rate of $\gamma \approx 2.4016$ and a angular frequency of $\omega \approx 201.034$.

The expected physical behavior in the linear regime (see, e.g., [9, 40]) is that the wave trades energy between the electric and magnetic field, while the amplitude of the field quantities decay in time. The energy lost from the fields is transferred to the kinetic energy of the plasma. In the following we will consider the electric energy

$$ee = \frac{1}{2C_P} \int \|(\partial_{xx} + \partial_{yy})\phi\|^2 d(x, y, z) \quad (19)$$

magnetic energy

$$me = \frac{1}{2C_A} \int \|(\partial_{xx} + \partial_{yy})A\|^2 d(x, y, z) \quad (20)$$

and the kinetic energy

$$ke = \frac{M_e}{2} \int v^2 f d(x, y, z, v).$$

We know that the total energy, i.e. $ee + me + ke$, is an invariant of equation (1). In addition, to the total energy, we will also consider the total mass

$$\int f d(x, y, z, v)$$

and the total momentum

$$\int v f d(x, y, z, v),$$

which are also invariants of the dynamics, in order to judge the quality of the numerical solution obtained. To compute the relative error for mass and energy we normalize with respect to the mass and energy of the initial value. The momentum is initially zero and we thus normalize with respect to $\int |v|f(0, x, y, z, v) d(x, y, z, v)$.

We first present numerical results using a solver that directly discretizes equation (1), henceforth called the full rank simulation. The results in Figure 1 show excellent agreement of the numerical solution compared to the decay rate and frequency predicted from linear theory, as we expect for the relatively small perturbation considered. We also use this simulation to investigate the low-rank structure of the simulation. To do that we perform a singular value decomposition for both f and E at each time step and plot the magnitude of the singular values. As we can see, from Figure 1, the dynamics is dominated by a single low-rank mode. Due to nonlinear effects some additional low-rank modes are excited. However, those are orders of magnitude smaller in magnitude than the dominant low-rank mode. Thus, the structure of the solution is inherently low-rank and can be well represented by such an approximation (as we would expect based on the discussion in section 4).

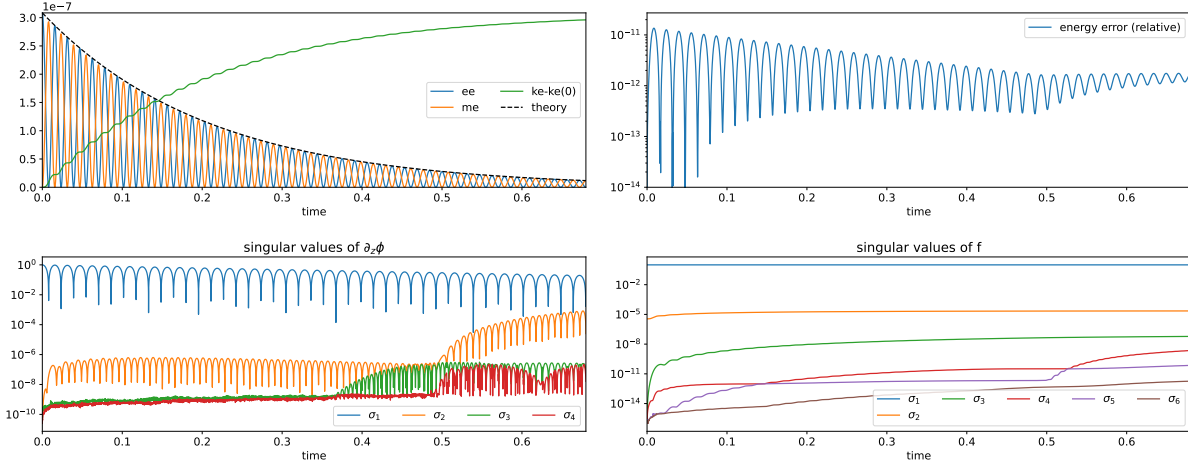


Figure 1: Numerical simulations of equation (1) with initial value given by equation (18) with $\beta/M_e = 1.8$ and $\alpha = 10^{-5}$ are shown. An FFT based direct (i.e. full rank) solver with time step size $\Delta t = 10^{-4}$ and 25, 25, 25, and 512 grid points in the x , y , z , and v direction, respectively, is used in all plots. On the top-left the time evolution of the electric energy, magnetic energy, and kinetic energy is shown. The analytic decay rate $\gamma \approx 2.4016$ is illustrated using a dashed black line. On the top right the violation of energy conservation by the algorithm is shown. On the bottom we show the magnitude of the dominant singular values for $\partial_z \phi$ (left) and the particle-density function f (right). All singular values are normalized with respect to the largest singular value at time $t = 0$.

We now consider the dynamical low-rank algorithm proposed in this paper. Details of the implementation and its computational efficiency will be discussed in section 6. We consider the same configuration as outlined above and simulations with fixed ranks $r = 2$ and $r = 5$ are conducted. The results are shown in Figure 2. We observe excellent agreement with the linear theory and with the full rank simulation. Moreover, the error in mass is close to machine precision and the error in momentum is below 10^{-10} . The error in energy, approximately 10^{-11} , has a similar magnitude than for the direct solver considered in Figure 1. This indicates that the space and time discretization has a more significant effect on the error in energy than the low-rank approximation. Thus we conclude that the dynamical low-rank algorithm, even at extremely small ranks such as $r = 2$, can obtain comparable results to the full rank simulation at drastically reduced computational and memory cost.

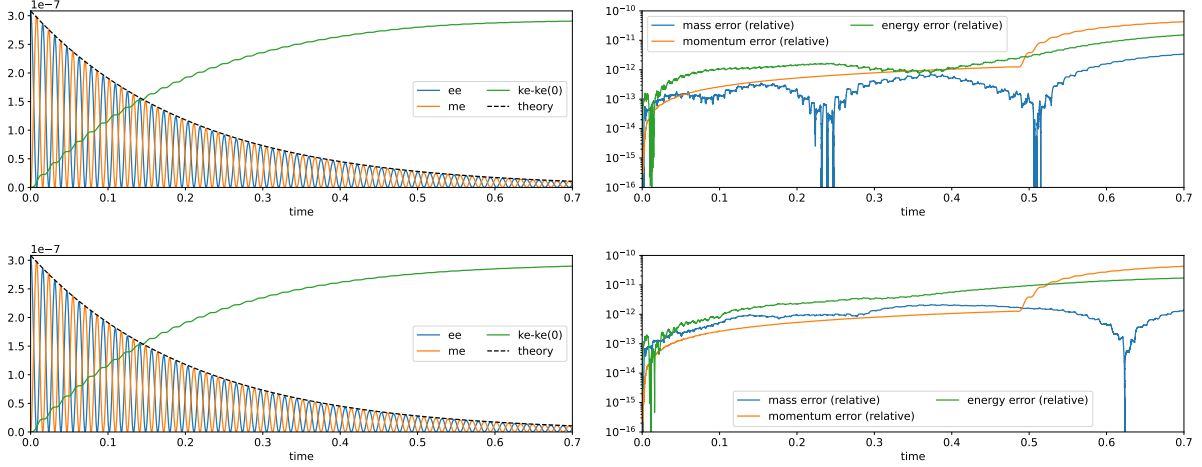


Figure 2: Numerical simulations of equation (1) with initial value given by equation (18) with $\beta/M_e = 1.8$ and $\alpha = 10^{-5}$ are shown. The dynamical low-rank Lie projector splitting with $r = 2$ (top) and $r = 5$ (bottom) is employed with an adaptive time step controller (the tolerance is set to 10^{-1}) and 32, 32, 32, and 512 grid points in the x , y , z , and v directions, respectively. On the left, the time evolution of the electric energy, magnetic energy, and kinetic energy is shown. The analytic decay rate $\gamma \approx 2.4016$ is illustrated using a dashed black line. The violation of mass, momentum, and energy conservation by the dynamical low-rank algorithm is shown on the right.

Second, we consider $\beta/M_e = 4$ and a significantly larger perturbation $\alpha = 10^{-2}$. From the full rank simulation in Figure 3 we observe an initial decay of the energy stored in the field quantities that matches the linear theory well. However, at approximately $t = 0.3$ nonlinear effects take over and the decay of the energy stored in the field quantities is stopped. These results match well with what has been reported in the literature (see, e.g. [40]); we note that for the present configuration and the used normalization the Alfvén time is $T_{\text{SAW}} = 2\pi/(v_A k_{\parallel}) = \sqrt{\beta} \approx 0.047$ and thus the simulation time covers approximately $15T_{\text{SAW}}$.

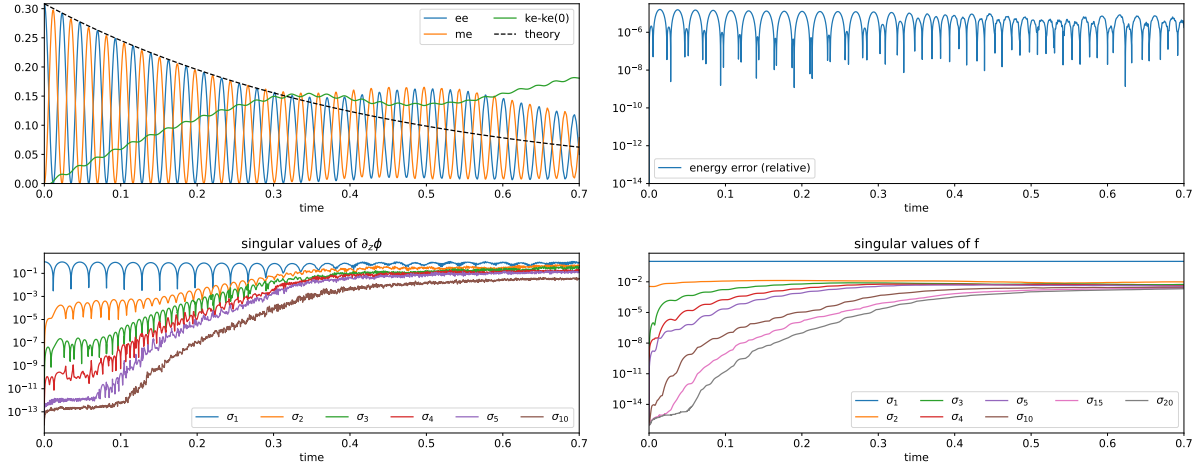


Figure 3: Numerical simulations of equation (1) with initial value given by equation (18) with $\beta/M_e = 4$ and $\alpha = 10^{-2}$ are shown. An FFT based direct (i.e. full rank) solver with time step size $\Delta t = 10^{-4}$ and 25, 25, 25, and 512 grid points in the x , y , z , and v direction, respectively, is used in all plots. On the top-left the time evolution of the electric energy, magnetic energy, and kinetic energy is shown. The analytic decay rate $\gamma \approx 1.1413$ is illustrated using a dashed black line. On the top right the violation of energy conservation by the algorithm is shown. On the bottom we show the magnitude of the dominant singular values for $\partial_z \phi$ (left) and the particle-density function f (right). All singular values are normalized with respect to the largest singular value at time $t = 0$.

We now turn our attention to the low-rank structure of the solution. Initially, the solution is dominated by a small number of low-rank modes, as we would expect in the regime where the linear theory holds. However, as time increases and nonlinear effects become more important, in addition to the dominant mode there is a multitude of low-rank modes with singular values with size approximately on the order of 10^{-2} . Thus, it is unclear how large the rank needs to be chosen in order to obtain a good approximation to the solution. In Figure 4 we did run the dynamical low-rank algorithm with rank $r = 3$, $r = 5$, $r = 8$, and $r = 10$. For rank $r = 3$ the results are at most qualitatively correct (we observe a wave with roughly the right frequency, but the amplitude is significantly larger than for the direct simulation). However, starting with rank $r = 5$ we obtain results that match the result from the full rank simulation very well. There is only a slight improvement going to rank $r = 8$. The simulation for $r = 8$ and $r = 10$ are almost indistinguishable. We also note that for all configurations the error in energy is of a similar magnitude as in the full rank simulation, suggesting that this error is dominated by the space and time discretization.

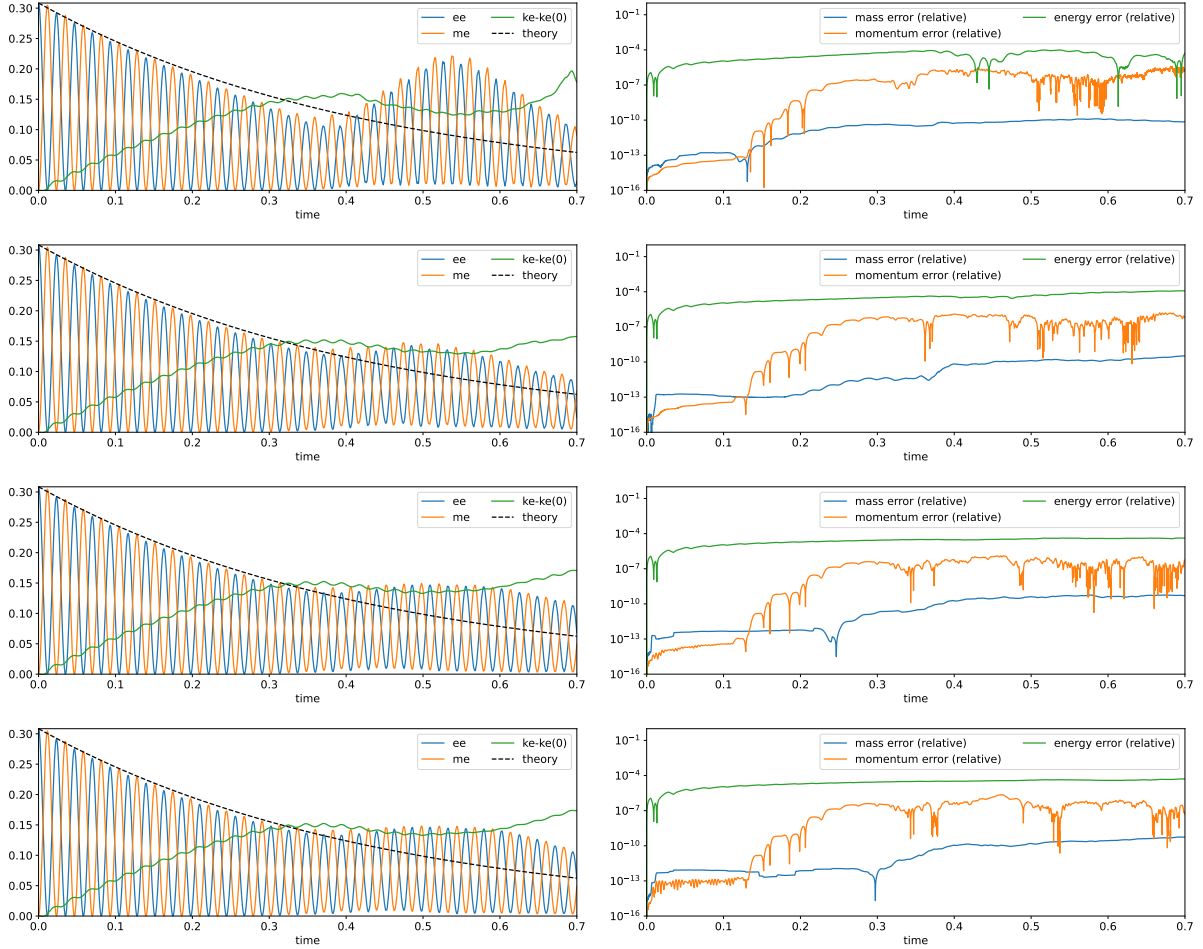


Figure 4: Numerical simulations of equation (1) with initial value given by equation (18) with $\beta/M_e = 4$ and $\alpha = 10^{-2}$ are shown. The Strang projector splitting dynamical low-rank approach proposed in this paper with (from top to bottom) $r = 3$, $r = 5$, $r = 8$, and $r = 10$ is employed with an adaptive time step controller (the tolerance is set to 10^{-1}) and 32, 32, 32, and 512 grid points in the x , y , z , and v directions, respectively. On the left the time evolution of the electric energy, magnetic energy, and kinetic energy is shown. The analytic decay rate $\gamma \approx 1.1413$ is illustrated using a dashed black line. The violation of mass, momentum, and energy conservation by the dynamical low-rank algorithm is shown on the right.

6. Comparison of numerical methods

In order to take the (continuous) dynamical low-rank approximation described in sections 3.1-3.3 and put it on a computer we have choose a robust integrator (see section 3.4) and perform a space and time discretization (see section 3.5). In this section we will consider how those choices effect computational performance. Our implementation of the dynamical low-rank algorithm is based on the open-source C++ framework Ensign [3]¹ and the code used in this paper and the corresponding unit tests can be found in the `examples` subfolder of that software package.

First, let us consider the choice of the robust integrator. We have three first order methods, the Lie projector splitting integrator (Algorithm 1), the BUG or unconventional integrator (Algorithm 2), and the augmented BUG integrator (Algorithm 3). We also consider the second order Strang projector splitting integrator (Algorithm 4). In Figure 5 we compare those four integrators for the configuration with $\beta/M_e = 1.8$ and $\alpha = 10^{-5}$ considered in the previous section. We employ the adaptive time stepping algorithm described in section 3.6. All integrators yield an electric and magnetic energy that matches the theoretical value and the full rank simulation well. Note, however, that the step size at which this is achieved is significantly different. For the second order Strang splitting we can take an (average) step size which is approximately a factor of 7 larger. Thus, more than making up for the fact that Strang splitting is approximately two times as costly as Lie splitting. As we would expect, conservation of the invariants, in particular, energy is also better for Strang splitting as compared to the other robust integrators. The Lie splitting scheme is approximately able to take the same time step size as the augmented BUG integrator, while being significantly less expensive (see Table 1, which we discuss in more detail later in this section).

¹Ensign is available at <https://github.com/leinkemmer/Ensign> under the MIT license.

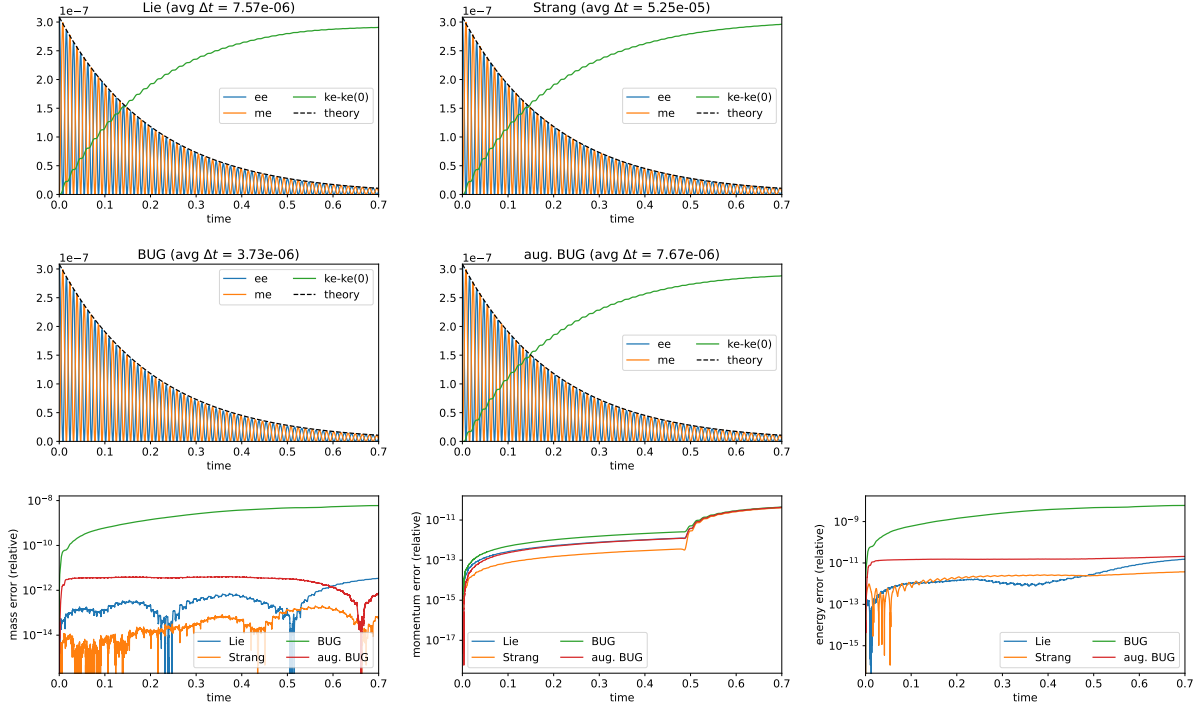


Figure 5: Time evolution of the electric, magnetic, and kinetic energy is shown for the Lie projector splitting (top-left), the Strang projector splitting (top-right), the BUG integrator (middle-left), and the augmented BUG integrator (middle-right). In all simulations the adaptive time stepping algorithm described in section 3.6 with a tolerance of 10^{-1} is used. On the bottom the error in mass (left), momentum (middle), and energy (right) committed by these methods is shown. The rank in all simulations is set to $r = 2$.

The outlier here is the BUG integrator. To obtain accurate results for the electric and magnetic energy we require more than twice as many time steps as for the first order projector splitting or the augmented BUG integrator. It also performs much worse with respect to mass and energy conservation (the error is approximately three orders of magnitude larger than for the projector splitting or the augmented BUG integrator).

To investigate this further we did run the three first order schemes with different fixed time step sizes. The result is shown in Figure 6 (the time step size decreases as we go from left to right). The most striking is that the BUG integrator actually decreases the kinetic energy instead of increasing it to balance out the reduction in electric and magnetic energy. This is a consequence of the bad energy conservation properties of that integrator that we observed earlier. Neither the projector splitting nor the augmented BUG integrator have this issue. As we increase the time step size both the projector splitting and the augmented BUG integrator become less accurate, as we would expect. However, for the largest time step size considered in Figure 6 the augmented BUG integrator becomes unstable, whereas the Lie projector splitting integrator still gives qualitatively correct.

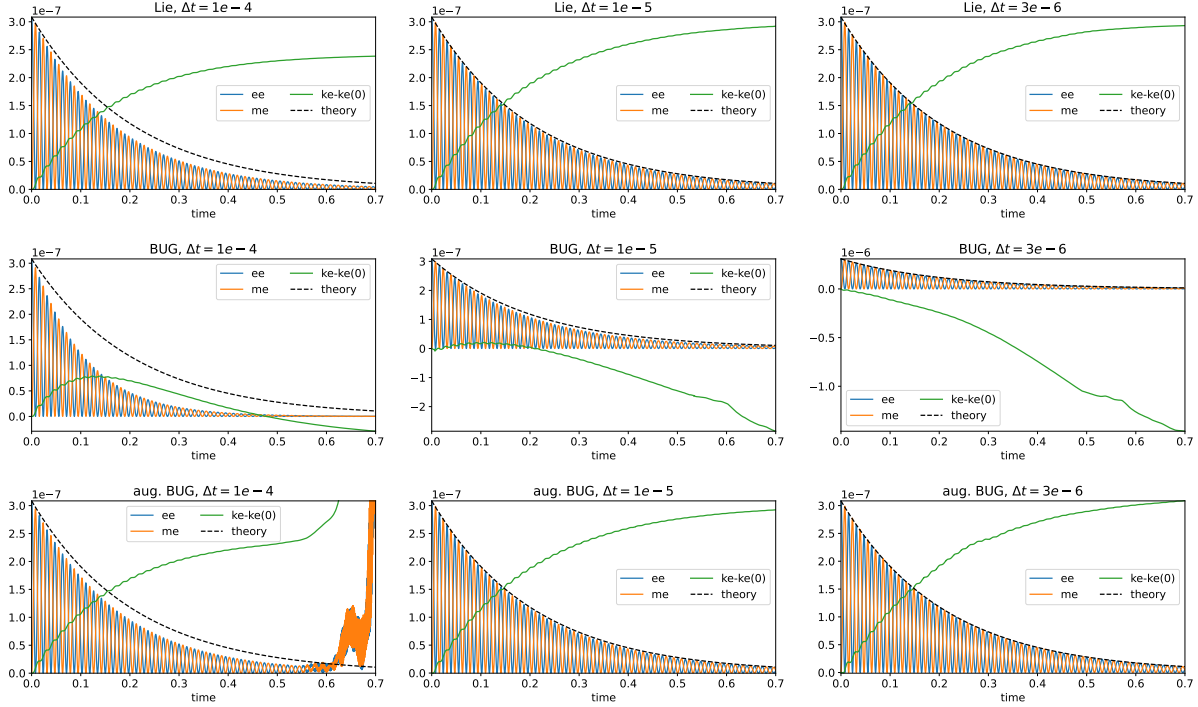


Figure 6: Time evolution of the electric, magnetic, and kinetic energy for the three first order integrators for three different fixed time step sizes is shown. Each column corresponds to a different time step size and each row corresponds to a different method. The rank in all simulations is set to $r = 5$.

Let us now consider the computational efficiency of the different low-rank algorithms. Both the run time for different configurations (i.e. different rank r and different spatial discretizations) as well as the memory consumption is shown in Table 1. We compare our C++ low-rank implementation to a direct (i.e. full rank) solver. The direct solver is implemented in Julia and thus this should not be entirely considered an apple to apple comparison. However, care has been taken in the Julia code to make it efficient by vectorizing the code. Since the direct solver is relatively easy to implement, primarily consisting of FFTs and vector operations, the performance of the code should not be too distant from a reasonable (but perhaps not highly optimized) C++ implementation. The low-rank code is written in C++ using the Ensign framework. Also in this case some care has been taken to obtain reasonable performance. In both cases we run the code sequentially on a dual socket Intel Gold 6130 system with 192 GB of RAM. The speedup obtained obviously depends on the rank of the simulation. For small ranks, e.g., $r = 5$ (as was a reasonable choice for all simulations considered in this paper), the speedup of the dynamical low-rank algorithm is dramatic. Even for relatively coarse grids (e.g. $32^3 \times 512$ or $64^3 \times 512$) the observed speedup is approximately three orders of magnitude. A similar reduction in memory is also observed. The latter is important as for fine grids (e.g. $256^3 \times 1024$) we can not even run the full rank simulation on a system with 192 GB of memory. However, even for $r = 15$ the dynamical low-rank algorithm only consumes approximately 60 MB of memory. Thus, the dynamical low-rank algorithms enables us to easily run simulations on a workstation or even laptop computer that would require supercomputer hardware and distributed memory parallelism otherwise.

Table 1 also contains a comparison of the different robust dynamical low-rank integrators. The Lie integrator is the cheapest overall, with the the BUG integrator following close behind (the primary additional cost in the BUG integrator is the recomputation of the coefficients in step 8 of Algorithm 2. The augmented BUG integrator is significantly more expensive. In fact, it is approximately equal in computational cost to the second order Strang projector splitting integrator. This is primarily due to the coefficients for the S step that need to be computed using rank $2r$. Overall, the Strang projector splitting integrators, which is between

two and three times as expensive as the Lie projector splitting integrator, gives the best performance. This is primarily due to the significantly increased time step size, as expected for a second order scheme (note that there is currently no second order variant of the BUG or augmented BUG integrator).

Resolution	rank	Lie (time/step)	BUG (time/step)	aug. BUG (time/step)	Strang (time/step)	speed up	memory usage	memory down
$32^3 \times 512$	full	29 s	–	–	–	–	0.27 GB	–
	2	0.013 s	0.015 s	0.02 s	0.035 s	2272	1 MB	512
	5	0.042 s	0.056 s	0.091 s	0.13 s	683	1 MB	205
	10	0.2 s	0.26 s	0.61 s	0.63 s	146	3 MB	102
	15	0.74 s	0.91 s	3.3 s	2.2 s	39	4 MB	68
$64^3 \times 512$	full	2.3e+02 s	–	–	–	–	2.1 GB	–
	2	0.024 s	0.038 s	0.043 s	0.075 s	9276	1 MB	2048
	5	0.13 s	0.16 s	0.26 s	0.35 s	1764	3 MB	819
	10	0.8 s	0.87 s	1.9 s	2 s	283	5 MB	410
	15	2.9 s	3 s	8 s	7 s	78	8 MB	273
$256^3 \times 1024$	full	–	–	–	–	–	2.7e+02 GB	–
	2	0.45 s	0.5 s	0.58 s	1.1 s	–	8 MB	32768
	5	4.1 s	4.2 s	6.7 s	9.2 s	–	21 MB	13107
	10	35 s	34 s	70 s	76 s	–	42 MB	6554
	15	1.7e+02 s	1.7e+02 s	4.4e+02 s	4.4e+02 s	–	63 MB	4369

Table 1: Timing result and memory consumption for the full rank simulation and the dynamical low-rank integrator for different values of the rank r and spatial resolutions. The speedup is computed using the Lie splitting as the full rank solution is also computed using a Lie splitting. The values for memory consumption are computed theoretically (for the full rank solution $2n_x n_y n_z n_v \text{sizeof}(\text{double})$ and for the low-rank algorithm $2r n_z n_v \text{sizeof}(\text{double})$), where n_x , n_y , n_z , and n_v are the number of points in the x , y , z , and v direction, respectively. The memory on our compute server was not sufficient to run the full problem using $256^3 \times 1024$ grid points.

Let us now turn our attention to the spatial and temporal discretization. In particular, we consider both a FFT based spectral discretization and a discretization based on the Lax–Wendroff scheme (both methods are described in detail in section 3.5). The corresponding numerical results are shown in Figure 7. Interestingly, the Lax–Wendroff scheme has a significantly lower error in momentum and a slightly lower overall error in energy. Otherwise, both methods give comparable results.

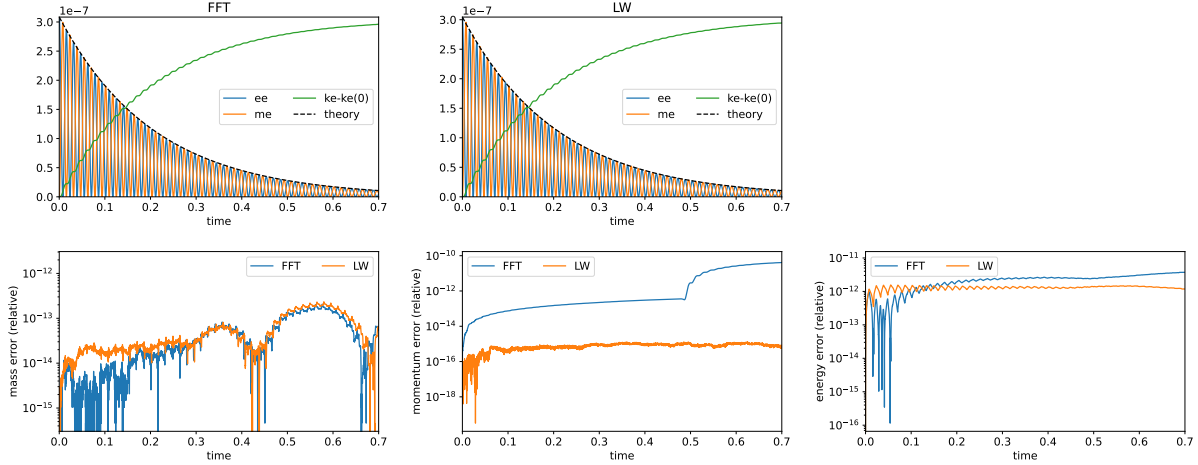


Figure 7: Time evolution of the electric, magnetic, and kinetic energy is shown for the Strang projector splitting scheme and the FFT based spectral discretization (top-left) and the Lax–Wendroff discretization (top-right). On the bottom the error in mass, momentum, and energy committed by these methods is shown. The rank in all simulations is set to $r = 2$.

References

- [1] F. Allmann-Rahn, R. Grauer, and K. Kormann. A parallel low-rank solver for the six-dimensional Vlasov–Maxwell equations. *J. Comput. Phys.*, 469:111562, 2022. doi: 10.1016/j.jcp.2022.111562.
- [2] M. Caliari, P. Kandolf, A. Ostermann, and S. Rainer. The Leja method revisited: Backward error analysis for the matrix exponential. *SIAM J. Sci. Comput.*, 38(3):A1639–A1661, 2016.
- [3] F. Cassini and L. Einkemmer. Efficient 6D Vlasov simulation using the dynamical low-rank framework Ensign. *Comput. Phys. Commun.*, 280:108489, 2022.
- [4] G. Ceruti and C. Lubich. Time integration of symmetric and anti-symmetric low-rank matrices and Tucker tensors. *BIT Numer. Math.*, 60:591–614, 2020.
- [5] G. Ceruti and C. Lubich. An unconventional robust integrator for dynamical low-rank approximation. *BIT Numer. Math.*, 62:23–44, 2022.
- [6] G. Ceruti, J. Kusch, and C. Lubich. A rank-adaptive robust integrator for dynamical low-rank approximation. *BIT Numer. Math.*, 62:1149–1174, 2022.
- [7] G. Ceruti, C. Lubich, and D. Sulz. Rank-adaptive time integration of tree tensor networks. *SIAM J. Numer. Anal.*, 61(1):194–222, 2023.
- [8] J. Coughlin and J. Hu. Efficient dynamical low-rank approximation for the Vlasov–Ampère–Fokker–Planck system. *J. Comput. Phys.*, 470:111590, 2022. doi: 10.1016/j.jcp.2022.111590.
- [9] T. Dannert and F. Jenko. Vlasov simulation of kinetic shear Alfvén waves. *Comput. Phys. Commun.*, 163(2):67–78, 2004. doi: 10.1016/j.cpc.2004.09.001.
- [10] P.J. Deka and L. Einkemmer. Exponential Integrators for Resistive Magnetohydrodynamics: Matrix-free Leja Interpolation and Efficient Adaptive Time Stepping. *Astrophys. J. Suppl. Ser.*, 259(2):57, 2022. doi: 10.3847/1538-4365/ac5177.
- [11] P.J. Deka and L. Einkemmer. Efficient adaptive step size control for exponential integrators. *Comput. Math. Appl.*, 123:59–74, 2022. doi: 10.1016/j.camwa.2022.07.011.

- [12] Z. Ding, L. Einkemmer, and Q. Li. Dynamical Low-Rank Integrator for the Linear Boltzmann Equation: Error Analysis in the Diffusion Limit. *SIAM J. Numer. Anal.*, 59(4), 2021.
- [13] S.P. Nørsett E. Hairer, G. Wanner. *Solving Ordinary Differential Equations I*. Springer, 1993. doi: 10.1007/978-3-540-78862-1.
- [14] V. Ehrlacher and D. Lombardi. A dynamical adaptive tensor method for the Vlasov–Poisson system. *J. Comput. Phys.*, 339:285–306, 2017.
- [15] L. Einkemmer. An adaptive step size controller for iterative implicit methods. *Appl. Numer. Math.*, 132:182–204, 2018. doi: 10.1016/j.apnum.2018.06.002.
- [16] L. Einkemmer. A low-rank algorithm for weakly compressible flow. *SIAM J. Sci. Comput.*, 41(5): A2795–A2814, 2019.
- [17] L. Einkemmer. A performance comparison of semi-Lagrangian discontinuous Galerkin and spline based Vlasov solvers in four dimensions. *Journal of Computational Physics*, 376:937–951, 2019.
- [18] L. Einkemmer and I. Joseph. A mass, momentum, and energy conservative dynamical low-rank scheme for the Vlasov equation. *J. Comput. Phys.*, 443:110495, 2021.
- [19] L. Einkemmer and C. Lubich. A low-rank projector-splitting integrator for the Vlasov–Poisson equation. *SIAM J. Sci. Comput.*, 40:B1330–B1360, 2018.
- [20] L. Einkemmer and A. Ostermann. An almost symmetric Strang splitting scheme for nonlinear evolution equations. *Comput. Math. with Appl.*, 67(12):2144–2157, 2014. doi: 10.1016/j.camwa.2014.02.027.
- [21] L. Einkemmer and A. Ostermann. An almost symmetric Strang splitting scheme for the construction of high order composition methods. *J. Comput. Appl. Math.*, 271:307–318, 2014. doi: 10.1016/j.cam.2014.04.015.
- [22] L. Einkemmer, A. Ostermann, and C. Piazzola. A low-rank projector-splitting integrator for the Vlasov–Maxwell equations with divergence correction. *J. Comput. Phys.*, 403:109063, 2020.
- [23] L. Einkemmer, J. Hu, and Y. Wang. An asymptotic-preserving dynamical low-rank method for the multi-scale multi-dimensional linear transport equation. *J. Comput. Phys.*, 439(110353), 2021.
- [24] L. Einkemmer, J. Hu, and L. Ying. An Efficient Dynamical Low-Rank Algorithm for the Boltzmann-BGK Equation Close to the Compressible Viscous Flow Regime. *SIAM J. Sci. Comput.*, 43(5):B1057–B1080, 2021. doi: 10.1137/21m1392772.
- [25] L. Einkemmer, A. Ostermann, and C. Scalone. A robust and conservative dynamical low-rank algorithm. *J. Comput. Phys.*, 484:112060, 2023.
- [26] V. Grandgirard, M. Brunetti, P. Bertrand, N. Besse, X. Garbet, P. Ghendrih, G. Manfredi, Y. Sarazin, O. Sauter, E. Sonnendrücker, J. Vaclavik, and L. Villard. A drift-kinetic Semi-Lagrangian 4D code for ion turbulence simulation. *J. Comput. Phys.*, 217(2):395–423, 2006. doi: <https://doi.org/10.1016/j.jcp.2006.01.023>.
- [27] W. Guo and J.-M. Qiu. A conservative low rank tensor method for the Vlasov dynamics. *arXiv:2201.10397*, 2022.
- [28] W. Guo and J.-M. Qiu. A low rank tensor representation of linear transport and nonlinear Vlasov solutions and their associated flow maps. *J. Comput. Phys.*, 458:111089, jun 2022. doi: 10.1016/j.jcp.2022.111089.
- [29] K. Gustafsson and G. Söderlind. Control strategies for the iterative solution of nonlinear equations in ODE solvers. *SIAM J. Sci. Comput.*, 18(1):23–40, 1997.

- [30] K. Gustafsson, M. Lundh, and G. Söderlind. A PI stepsize control for the numerical solution of ordinary differential equations. *BIT Numer. Math.*, 28(2):270–287, 1988.
- [31] A. Hasegawa and M. Wakatani. Plasma Edge Turbulence. *Phys. Rev. Lett.*, 50(9):682–686, 1983. doi: 10.1103/physrevlett.50.682.
- [32] C. Hauck and S. Schnake. A Predictor-Corrector Strategy for Adaptivity in Dynamical Low-Rank Approximations. *arXiv:2209.00550*, 2022.
- [33] M. Hochbruck, M. Neher, and S. Schrammer. Rank-adaptive dynamical low-rank integrators for first-order and second-order matrix differential equations. *BIT Numer. Math.*, 63(1), 2023. doi: 10.1007/s10543-023-00942-6.
- [34] T. Jahnke and W. Huisinga. A dynamical low-rank approach to the chemical master equation. *Bull. Math. Biol.*, 70(8):2283–2302, 2008. doi: 10.1007/s11538-008-9346-x.
- [35] O. Koch and C. Lubich. Dynamical low-rank approximation. *SIAM J. Matrix Anal. Appl.*, 29:434–454, 2007. doi: 10.1137/050639703.
- [36] K. Kormann. A semi-Lagrangian Vlasov solver in tensor train format. *SIAM J. Sci. Comput.*, 37: 613–632, 2015. doi: 10.1137/140971270.
- [37] J. Kusch and P. Stammer. A robust collision source method for rank adaptive dynamical low-rank approximation in radiation therapy. *arXiv:2111.07160*, 2021.
- [38] J. Kusch, L. Einkemmer, and G. Ceruti. On the Stability of Robust Dynamical Low-Rank Approximations for Hyperbolic Problems. *SIAM J. Sci. Comput.*, 45(1):A1–A24, 2023. doi: 10.1137/21m1446289.
- [39] G. Latu, V. Grandgirard, J. Abiteboul, N. Crouseilles, G. Dif-Pradalier, X. Garbet, P. Ghendrih, M. Mehrenberger, Y. Sarazin, and E. Sonnendrücker. Improving conservation properties in a 5D gyrokinetic semi-Lagrangian code. *Eur. Phys. J. D*, 68, 2014. doi: 10.1140/epjd/e2014-50209-1.
- [40] Z.X. Lu, G. Meng, M. Hoelzl, and P. Lauber. The development of an implicit full f method for electromagnetic particle simulations of Alfvén waves and energetic particle physics. *J. Comput. Phys.*, 440: 110384, 2021. doi: 10.1016/j.jcp.2021.110384.
- [41] C. Lubich. *From quantum to classical molecular dynamics: reduced models and numerical analysis*. European Mathematical Society, Zürich, 2008.
- [42] C. Lubich and I.V. Oseledets. A projector-splitting integrator for dynamical low-rank approximation. *BIT Numer. Math.*, 54:171–188, 2014. doi: 10.1007/s10543-013-0454-0.
- [43] C. Lubich, T. Rohwedder, R. Schneider, and B. Vandereycken. Dynamical approximation by hierarchical Tucker and tensor-train tensors. *SIAM J. Matrix Anal. Appl.*, 34:470–494, 2013.
- [44] C. Lubich, I.V. Oseledets, and B. Vandereycken. Time integration of tensor trains. *SIAM J. Numer. Anal.*, 53:917–941, 2015.
- [45] C. Lubich, B. Vandereycken, and H. Walach. Time integration of rank-constrained Tucker tensors. *SIAM J. Numer. Anal.*, 56:1273–1290, 2018.
- [46] H.-D. Meyer, F. Gatti, and G. A. Worth. *Multidimensional quantum dynamics*. John Wiley & Sons, 2009.
- [47] A. Nonnenmacher and C. Lubich. Dynamical low-rank approximation: applications and numerical experiments. *Math. Comput. Simul.*, 79(4):1346–1357, 2008.

- [48] Z. Peng and R. McClarren. A high-order/low-order (HOLO) algorithm for preserving conservation in time-dependent low-rank transport calculations. *J. Comput. Phys.*, 447(110672), 2021.
- [49] Z. Peng, R. McClarren, and M. Frank. A low-rank method for two-dimensional time-dependent radiation transport calculations. *J. Comput. Phys.*, 421(109735), 2020.
- [50] M. Prugger, L. Einkemmer, and C.F. Lopez. A dynamical low-rank approach to solve the chemical master equation for biological reaction networks. *J. Comput. Phys.*, page 112250, 2023. doi: 10.1016/j.jcp.2023.112250.
- [51] E. Sonnendrücker, J. Roche, P. Bertrand, and A. Ghizzo. The semi-Lagrangian method for the numerical resolution of the Vlasov equation. *J. Comput. Phys.*, 149(2):201–220, 1999.
- [52] J. P. Verboncoeur. Particle simulation of plasmas: review and advances. *Plasma Phys. Control. Fusion*, 47(5A):A231, 2005.

Appendix A. Dispersion relation

Taking Fourier transforms in time and physical space, i.e. $u(t, x) = \sum_{\omega k} \hat{u}_{\omega k} e^{ik \cdot x - i\omega t}$, we get from equation (14)

$$-i\omega \hat{f}_{\omega k} + ik_{\parallel} v \hat{f}_{\omega k} + \frac{1}{M_e} \left[ik_{\parallel} \hat{\phi}_{\omega k} \partial_v f_{eq} - i\omega \hat{A}_{\omega k} \partial_v f_{eq} \right] = 0 \quad (\text{A.1})$$

$$k_{\perp}^2 \hat{\phi}_{\omega k} = C_P \int \hat{f}_{\omega k} dv, \quad (\text{A.2})$$

$$k_{\perp}^2 \hat{A}_{\omega k} = C_A \int v \hat{f}_{\omega k} dv, \quad (\text{A.3})$$

where $k_{\perp}^2 = k_1^2 + k_2^2$ and $k_{\parallel} = k_3$. Since in this linear theory all the Fourier modes decouple we, from now on, will suppress the indices ω and k .

Plugging equations (A.2) and (A.3) into equation (A.1) we get

$$i(-\omega + k_{\parallel} v) \hat{f} + \frac{ik_{\parallel} C_P}{k_{\perp}^2 M_e} (\partial_v f_{eq}) \left(\int \hat{f} dv \right) - \frac{i\omega C_A}{k_{\perp}^2 M_e} (\partial_v f_{eq}) \left(\int v \hat{f} dv \right) = 0$$

and thus

$$\hat{f} - \frac{C_P k_{\parallel}}{M_e k_{\perp}^2} \frac{1}{k_{\parallel} v - \omega} (\partial_v f_{eq}) \left(\int \hat{f} dv \right) + \frac{C_A \omega}{M_e k_{\perp}^2} \frac{1}{k_{\parallel} v - \omega} (\partial_v f_{eq}) \left(\int v \hat{f} dv \right) = 0.$$

We can now express $\int v \hat{f} dv$ using $\int \hat{f} dv$ by using the continuity equation

$$\partial_t \int f dv + \partial_z \int v f dv = 0.$$

In frequency space we have

$$-i\omega \int \hat{f} dv + ik \int v \hat{f} dv = 0$$

and thus

$$\int v \hat{f} dv = \frac{\omega}{k_{\parallel}} \int \hat{f} dv.$$

We then have

$$\hat{f} - \left[\frac{C_P k_{\parallel}}{M_e k_{\perp}^2} \frac{1}{k_{\parallel} v - \omega} + \frac{C_A \omega}{M_e k_{\perp}^2} \frac{\omega/k_{\parallel}}{k_{\parallel} v - \omega} \right] (\partial_v f_{eq}) \left(\int \hat{f} dv \right) = 0$$

By integrating in v we obtain

$$\left[1 - \left(\frac{C_P}{M_e} \frac{k_{\parallel}}{k_{\perp}^2} - \frac{C_A}{M_e} \frac{\omega^2}{k_{\perp}^2 k_{\parallel}} \right) \int \frac{\partial_v f_{eq}}{k_{\parallel} v - \omega} dv \right] \int \hat{f} dv = 0$$

from which we get

$$1 - \frac{1 - \beta\omega^2/k_{\parallel}^2}{M_e (k_{\perp} \bar{\rho}_i)^2} \int \frac{\partial_v f_{eq}}{v - \omega/k_{\parallel}} dv = 0,$$

where $\bar{\rho}_i = \rho_i/L$.

In order to being able to evaluate the integral we have to specify f_{eq} . We will use a Maxwellian here, i.e.

$$f_{eq} = \frac{\exp(-v^2/v_{th,e}^2)}{\sqrt{\pi} v_{th,e}} = \sqrt{\frac{M_e}{\pi}} \exp(-M_e v^2),$$

since $v_{th,e} = \sqrt{2T_{ref}/m_e} = v_{th,i}/\sqrt{M_e} = 1/\sqrt{M_e}$ (remember that we express velocities in units of $v_{th,i}$). It is useful to introduce $\bar{\omega} = \omega/(v_{th,e} k_{\parallel}) = \sqrt{M_e} \omega/k_{\parallel}$. Then

$$\int \frac{\partial_v f_{eq}}{v - \omega/k_{\parallel}} dv = -M_e \int \frac{2v\sqrt{M_e} f_{eq}(v)}{v\sqrt{M_e} - \sqrt{M_e}\omega/k_{\parallel}} dv.$$

Substituting $u = v\sqrt{M_e}$ we get

$$\begin{aligned} \int \frac{\partial_v f_{eq}}{v - \omega/k_{\parallel}} dv &= -M_e \int \frac{2u f_{eq}(u/\sqrt{M_e})}{u - \bar{\omega}} du \\ &= -2M_e [1 + \bar{\omega} Z(\bar{\omega})], \end{aligned}$$

where

$$Z(a) = \frac{1}{\sqrt{\pi}} \int \frac{e^{-v^2}}{v - a} dv = i\sqrt{\pi} e^{-a^2} (1 + \operatorname{erf}(ia)).$$

We thus have

$$1 - \frac{2[1 + \bar{\omega} Z(\bar{\omega})]}{(k_{\perp} \bar{\rho}_i)^2} (\beta\omega^2/k_{\parallel}^2 - 1) = 0$$

and therefore we get the dispersion relation

$$1 - \frac{2[1 + \bar{\omega} Z(\bar{\omega})]}{(k_{\perp} \bar{\rho}_i)^2} (\beta/M_e \bar{\omega}^2 - 1) = 0$$

The two dimensionless parameters that determine $\bar{\omega}$ here are β/M_e and $k_{\perp} \bar{\rho}_i$.